[3] Y. Nikawa, N. Hoshi, K. Yamamoto, and K. Kikuchi, "Microwave heating using pulse modulated waves," in *Proc. 6th Int. Microwave High-Freq. Heating Conf.*, Fermo, Italy, Sept. 7–13, 1997, pp. 357–360.

Time-Varying Volterra-Series Analysis of Spectral Regrowth and Noise Power Ratio in FET Mixers

J. Angel García, M. L. De la Fuente, J. Carlos Pedro, N. B. Carvalho, Y. Newport, A. Mediavilla, and A. Tazón

***Abstract*—This paper presents a direct and robust analysis technique for evaluating nonlinear distortion phenomena in FET mixers excited by multitone signals. Time-varying Volterra-series analysis has previously been proven to be appropriate for small-signal intermodulation-distortion calculations in mixers excited by simple RF signals. Spectral convolutions of the suitably mapped control voltages are introduced in this paper in order to solve the nonlinear current source calculations for narrow-band modulated or broad-band multicarrier RF signals. Simulations and measurements of a properly characterized resistive mixer validate the accuracy of this direct and noniterative analysis tool for spectral regrowth and noise-power-ratio prediction in such applications.**

***Index Terms*—Intermodulation distortion, MESFETs, mixers, Volterra series.**

I. Introduction

The complex nature of the nonlinear distortion phenomena appearing in microwave applications, when excited by multitone signals, has determined an increased use of new characterization procedures instead of the classical two-tone intermodulation distortion (IMD) test. In this sense, the adjacent channel power ratio (ACPR) is being widely employed for evaluating the broadening of a signal bandwidth (spectral regrowth) and the distortion caused in the neighbor signals. The noise power ratio (NPR) is, however, preferred to quantify the total co-channel distortion appearing in a particular frequency band of a multicarrier signal.

In amplifiers, this problem has recently been considered making use of low-frequency transformations [1], transient envelope analysis [2], Volterra series [3], or spectral balance [4]. However, very few results have been reported for other applications [5], and the mixer case is as yet unsolved. For small-signal RF excitations, the case of most practical significance in mixers, time-varying Volterra-series analysis has been proven to constitute an accurate and simple tool for IMD calculations [6]. Nevertheless, and to the authors' knowledge, most published works in FET mixers have dealt with simple (one- or two-tone) RF signals [7], [8].

In this paper, we propose a technique to extend this powerful nonlinear analysis method to the handling of more complex excitation signals at circuit level. In an analogous way to [3], it is assumed that the circuit is weakly nonlinear for the RF signal such that a time-varying Taylor-series expansion of the device's nonlinearities up to the third degree is adequate. The accuracy of our approach is validated comparing measured and simulated values in a resistive mixer in a previously unpublished way.

Manuscript received August 27, 1999.

J. A. García is with TTI Norte, 39005 Santander, Spain (e-mail: jangel@ieee.org).

M. L. De la Fuente, Y. Newport, A. Mediavilla, and A. Tazón are with the Department Ingeniería de Comunicaciones, Universidad de Cantabria, 39005 Santander, Spain.

J. C. Pedro and N. B. Carvalho are with the Instituto de Telecomunicações, 3810 Aveiro, Portugal.

Publisher Item Identifier S 0018-9480(01)01691-X.

II. Time-Varying Volterra Analysis

The time-varying Volterra-series or large-signal/small-signal technique [9] begins by first analyzing the nonlinear circuit under large-signal excitation (LO), employing, for instance, the well-known harmonic-balance method. The nonlinear circuit components are then replaced by time-varying elements, and the small-signal nonlinear current technique of Volterra-series applied.

In Fig. 1, we show the general topology of a single FET mixer for applying the above technique. In active gate or drain mixers, $V_{\rm RF} = V{\rm g}$ represents the RF signal, a role played by $V{\rm d}$ if it is resistive. The circuit has been divided into a linear subcircuit where the elements have been represented by their conversion matrices, and the nonlinear current sources ($I{\rm gs}_i^{\rm NL}$, $I{\rm gd}_i^{\rm NL}$, and $I{\rm ds}_i^{\rm NL}$) determined by the ith degree Taylor expansion terms ($i > 1$) for each respective nonlinearity. The subindex c indicates the conversion matrix for the corresponding time-varying element, Ω and "1" represent the frequency diagonal and identity matrices [9]. Impedance matrices are used for the inductances, while the admittance ones describe the capacitances.

Solving the linear subcircuit to obtain the first-order control voltages and the first-order parameters (conversion loss or gain, RF input impedance, and IF output impedance) for a discrete multitone excitation, or a discretized continuous spectrum, does not differ in principle from the classical one- or two-tone case. The conversion matrices should be evaluated, and the circuit solved for each excitation frequency component.

The problem arises when the nonlinear current sources have to be evaluated. To illustrate this situation, we will consider the second-order nonlinear current source for the predominant nonlinearity $I{\rm ds}(V{\rm gs}, V{\rm ds})$, whose Taylor-series expansion is represented in the following:

$$\begin{aligned} I{\rm ds}(V{\rm gs}, V{\rm ds}) = {} & I{\rm ds}(V_{\rm GS}, V_{\rm DS}) + Gm1 \cdot v{\rm gs} + Gds \cdot v{\rm ds} \\ & + Gm2 \cdot v{\rm gs}^2 + Gmd \cdot v{\rm gs} \cdot v{\rm ds} + Gd2 \cdot v{\rm ds}^2 \\ & + Gm3 \cdot v{\rm gs}^3 + Gm2d \cdot v{\rm gs}^2 \cdot v{\rm ds} \\ & + Gmd2 \cdot v{\rm gs} \cdot v{\rm ds}^2 + Gd3 \cdot v{\rm ds}^3. \end{aligned} \tag{1}$$

From the first-order calculation, we can obtain a set of first-order control voltages $V{\rm gs}_1$ and $V{\rm ds}_1$. Each control voltage vector would be of the form

$$V{\rm gs}_1(\Omega_k) = \begin{bmatrix} V{\rm gs}_1^{-N}(N \cdot \omega_{\rm LO} - \omega_k)^* \\ \vdots \\ V{\rm gs}_1^{-1}(\omega_{\rm LO} - \omega_k)^* \\ V{\rm gs}_1^{0}(\omega_k) \\ V{\rm gs}_1^{1}(\omega_{\rm LO} + \omega_k) \\ \vdots \\ V{\rm gs}_1^{N}(N \cdot \omega_{\rm LO} + \omega_k) \end{bmatrix}, \quad \text{with } \omega_k = |\omega_{\rm LO} - \omega_{{\rm RF}_k}| \quad \text{and } k = 1, \cdots, K. \tag{2}$$

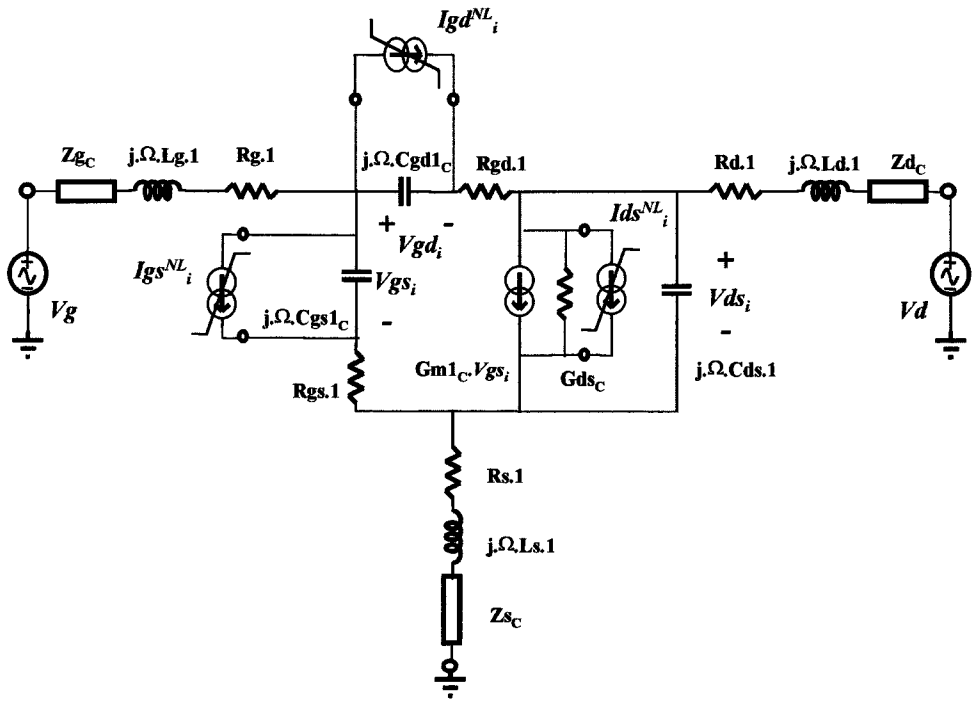

Fig. 1. Single FET mixer equivalent circuit for applying time-varying nonlinear current technique.

K represents the number of discrete excitation tones, and N the number of LO harmonics to be considered. The upper part of the vector contains the conjugate values of the phasors representing the lower sidebands, while the lower part represents the values for the upper sidebands, as in [9]. If the excitation tones are uniformly spaced in frequency, then $\omega_k = \omega_{k=1} + (k-1)\cdot\Delta\omega$ with $k = 1, \ldots, K$ and $\Delta\omega$ the frequency step.

In time domain, the second-order nonlinear current source would be determined by the second-order Taylor coefficients and the first-order control voltages as in (3)

$$i\mathrm{ds}_2^{\mathrm{NL}}(t) = Gm2(t)\cdot v\mathrm{gs}_1^2(t) + Gmd(t)\cdot v\mathrm{gs}_1(t)\cdot v\mathrm{ds}_1(t) + Gd2(t)\cdot v\mathrm{ds}_1^2(t). \quad (3)$$

A time-domain product becomes a frequency-domain convolution, resulting in (4)

$$I\mathrm{ds}_2^{\mathrm{NL}}(\omega) = Gm2(\omega) * V\mathrm{gs}_1(\omega) * V\mathrm{gs}_1(\omega) + Gmd(\omega) * V\mathrm{gs}_1(\omega) * V\mathrm{ds}_1(\omega) + Gd2(\omega) * V\mathrm{ds}_1(\omega) * V\mathrm{ds}_1(\omega). \quad (4)$$

The relation between the calculated first-order vectors and their corresponding position in the spectrum can be visualized in Fig. 2. It is quite evident that a spectrum of this kind with the real frequency variable would be quite sparse and difficult to handle in a convolution product. However, the frequency-domain nature of Volterra analysis lets us compress such sparse spectrum without affecting the convolution result [10]. In spite of the minimum separation necessary between clusters or bands, to avoid aliasing when the convolutions are evaluated, the computational efforts are greatly reduced.

Once we have made the convolution, two definite second-order frequency-band sets appear, a difference and a sum band set. Two sets of vectors corresponding to each second-order frequency component in the difference and sum bands can be obtained, as shown in Fig. 3. This is not a difficult task thanks to the previous knowledge we have of the second-order real values for the frequency components appearing in the compressed or mapped convolution. These second-order vectors are shown in (5) for the $V\mathrm{gs}_1 * V\mathrm{gs}_1$ convolution in (4) as follows:

$$V\mathrm{gs}_2(\Omega_s)_{\mathrm{Sum}} = \begin{bmatrix} V\mathrm{gs}_2^{-N}(N\cdot\omega_{\mathrm{LO}} - \omega_s)^* \\ \vdots \\ V\mathrm{gs}_2^{-1}(\omega_{\mathrm{LO}} - \omega_s)^* \\ V\mathrm{gs}_2^{0}(\omega_s) \\ V\mathrm{gs}_2^{1}(\omega_{\mathrm{LO}} + \omega_s) \\ \vdots \\ V\mathrm{gs}_2^{N}(N\cdot\omega_{\mathrm{LO}} + \omega_s) \end{bmatrix}_{\mathrm{Sum}},$$
$$\text{with } \omega_s = 2\cdot\omega_{k=1} + (s-1)\cdot\Delta\omega;$$
$$s = 1, \ldots, 2K-1$$

$$V\mathrm{gs}_2(\Omega_d)_{\mathrm{Dif}} = \begin{bmatrix} V\mathrm{gs}_2^{-N}(N\cdot\omega_{\mathrm{LO}} - \omega_d)^* \\ \vdots \\ V\mathrm{gs}_2^{-1}(\omega_{\mathrm{LO}} - \omega_d)^* \\ V\mathrm{gs}_2^{0}(\omega_d) \\ V\mathrm{gs}_2^{1}(\omega_{\mathrm{LO}} + \omega_d) \\ \vdots \\ V\mathrm{gs}_2^{N}(N\cdot\omega_{\mathrm{LO}} + \omega_d) \end{bmatrix}_{\mathrm{Dif}},$$
$$\text{with } \omega_d = (d-1)\cdot\Delta\omega;$$
$$d = 1, \ldots, K. \quad (5)$$

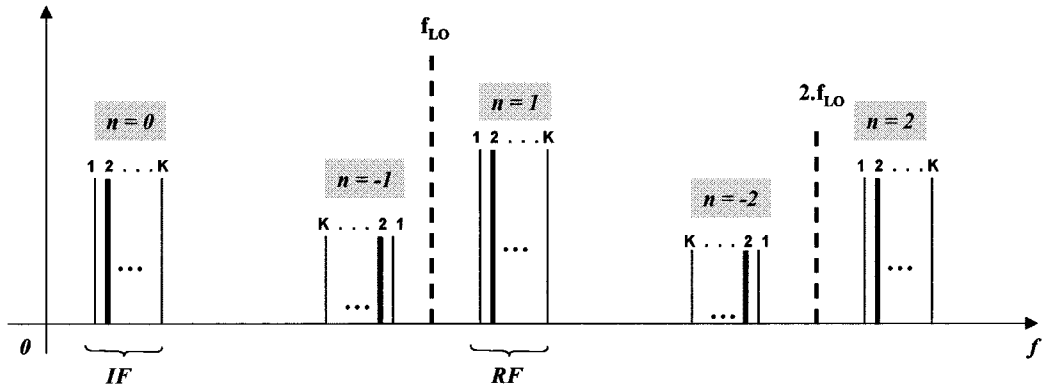

Fig. 2. Spectrum of a first-order control voltage for a K-tone RF excitation and considering $N = 2$ LO harmonics. The components of the vector for $k = 2$ have been represented with broad lines.

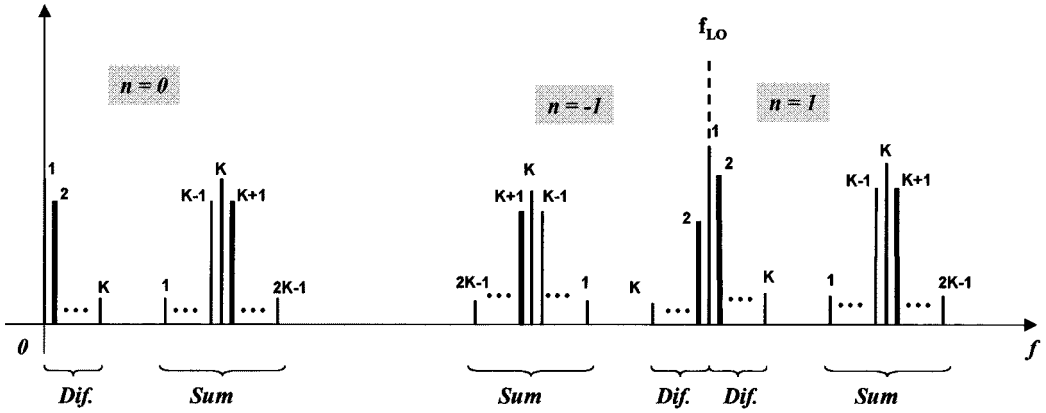

Fig. 3. Spectrum of a second-order control voltage for a K-tone RF excitation and considering an $N = 1$ LO harmonic. The components of the difference vector for $d = 2$ and the sum vector for $s = K + 1$ have been represented with broad lines.

The convolution of the LO time-varying second-degree coefficient in (3) with the resulting control voltage convolution can be reduced to a simple multiplication of the corresponding conversion matrix and each member of the set of second-order control voltage vectors. The corresponding set of vectors for the second-order nonlinear current source would be then evaluated as in (6) for both the sum and difference bands, and for each second-order k component

$$I\mathrm{ds}_{2_{\mathrm{Band}}}^{\mathrm{NL}} = Gm2_C \cdot V\mathrm{gs}_{2_{\mathrm{Band}}} + Gmd_C \cdot V\mathrm{gsds}_{2_{\mathrm{Band}}} + Gd2_C \cdot V\mathrm{ds}_{2_{\mathrm{Band}}} \quad (6)$$

where $V\mathrm{gsds}_{2_{\mathrm{Band}}}$ and $V\mathrm{ds}_{2_{\mathrm{Band}}}$ constitute sets of vectors as in (5), but representing the results from the $V\mathrm{gs}_1 * V\mathrm{ds}_1$ and $V\mathrm{ds}_1 * V\mathrm{ds}_1$ convolutions in corresponding order ($\mathrm{Band} = \mathrm{Sum}, \mathrm{Dif}$).

The situation is analogously repeated for the third-order case. Two definite sets of third-order frequency bands appear, one of these is centered in the first-order bands and defines the in-band distortion phenomena we are interested in.

III. Spectral Regrowth and NPR Results

The proposed technique for calculating the nonlinear current sources was included in an in-house time-varying Volterra-series simulator [11] to evaluate spectral regrowth and NPR in single FET mixer structures. For illustrative purposes, a resistive mixer employing a 6×50 μm F20 MESFET from GEC-Marconi, Caswell, U.K., was designed, measured, and simulated under multitone excitation.

As accurate nonlinear distortion calculations in a mixer also require the reproduction of the nonlinearity derivatives throughout the LO excursion, we made a careful extraction of the coefficients in (1) in the whole linear region as in [11].

A. Spectral Regrowth

In Fig. 4, we show the RF input spectrum as well as the simulated and measured values of the spectral regrowth appearing at the IF. The LO signal was located at 1.6 GHz and had an available power of 0 dBm. The multitone RF excitation was created by modulating a 1.7-GHz carrier with a 2-MHz bandwidth deterministic baseband signal. The modulation format was QPSK. The input spectrum was discretized in 61 components whose phase relation was available. Such a large number of tones can be handled without problem thanks to the noniterative nature of the Volterra-series approach. As can be appreciated, there is a very good agreement between both sets of results.

B. NPR

In Fig. 5, we represent the RF input and IF output spectrum for an NPR experiment. For the simulation, a discrete amplitude spectrum was generated from the NPR excitation, and different calculation results for correspondent random phase distributions were evaluated

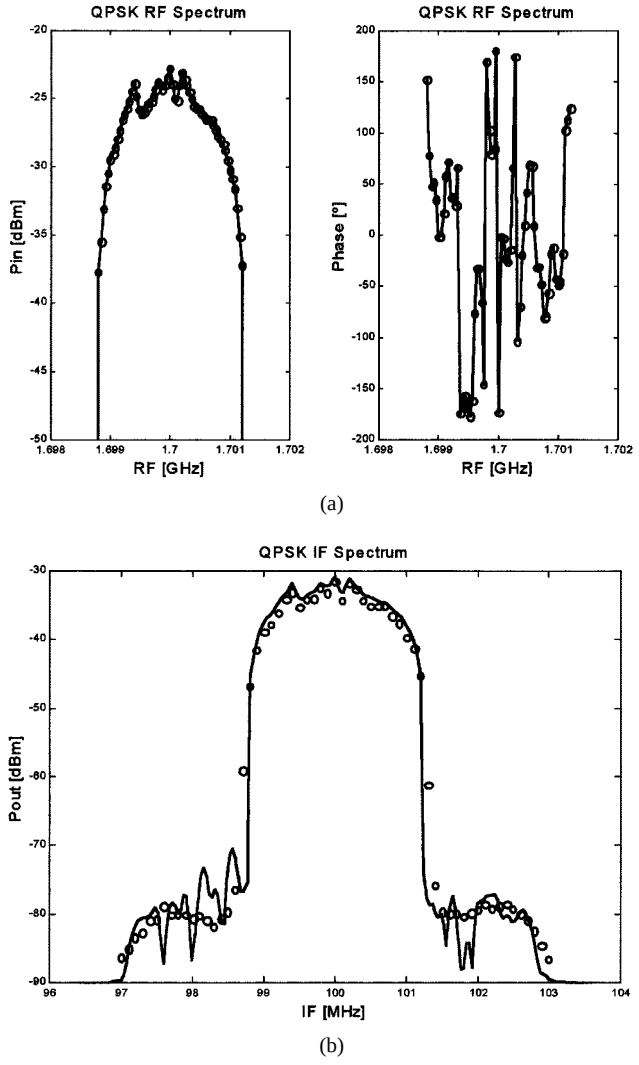

Fig. 4. Spectral regrowth prediction. (a) RF input amplitude and phase discretized spectrum. (b) Simulated (—) and measured (ooo) IF output amplitude spectrum.

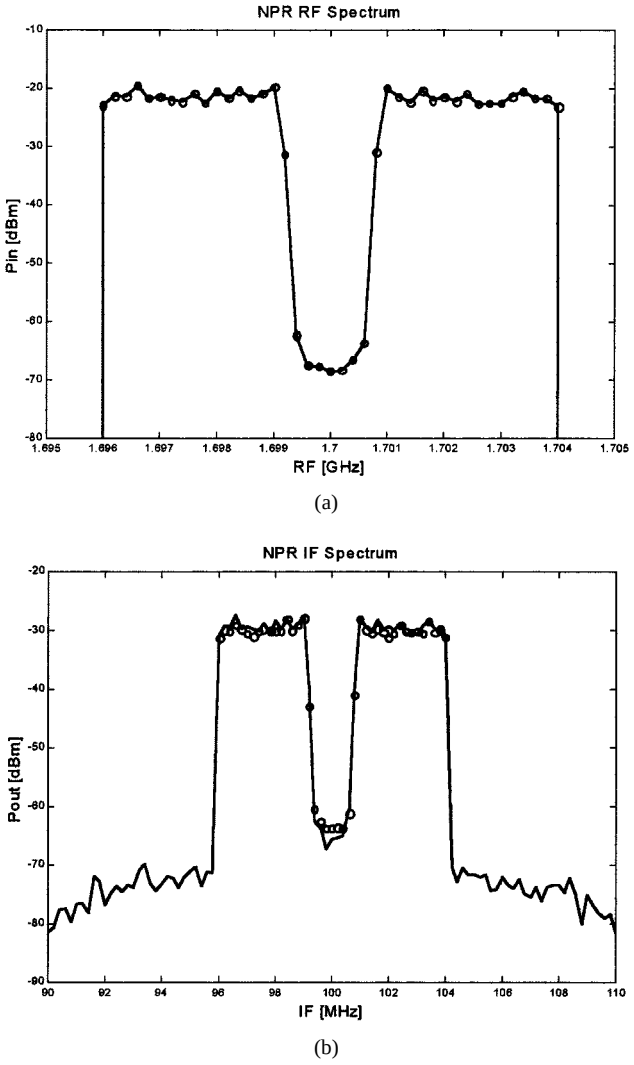

Fig. 5. NPR prediction. (a) RF input amplitude discretized spectrum. (b) Simulated (—) and measured (ooo) IF output amplitude spectrum.

and averaged. Once again, the direct nature of Volterra-series calculations lets us employ a small frequency interval when discretizing the spectrum. This gives rise to a large number of frequency components and, thus, a situation closer to the original continuous NPR spectrum than the one reproduced by other frequency-domain techniques. It also enables the possibility of evaluating and averaging different phase distributions without the computational effort required in others. The predictions are quite similar to the measurements, validating our approach.

IV. Conclusions

It has been shown that small-signal nonlinear distortion phenomena, such as spectral regrowth and NPR, can be efficiently predicted in FET mixers employing time-varying Volterra-series analysis with mapped frequency convolutions and an adequate device model. As the RF signal is handled in the second part of the method, its direct and noniterative nature, as well as the absence of time–frequency domain transformations, determines a high degree of accuracy and the absence of convergence problems. The method is not limited to narrow-band signals. If necessary, the RF small-signal amplitude limitation can be relaxed if the analysis is extended to fifth or even seventh order, but at the expense of a great increase in computational effort.

References

[1] J. S. Kenney and A. Leke, "Power amplifier spectral regrowth for digital cellular and PCS applications," *Microwave J.*, vol. 38, no. 10, pp. 74–92, Oct. 1995.

[2] E. Ngoya and R. Larchevèque, "Envelope transient analysis: A new method for the transient and steady state analysis of microwave communication circuits and systems," in *IEEE MTT-S Int. Microwave Symp. Dig.*, 1996, pp. 1365–1368.

[3] S. A. Maas, "Volterra analysis of spectral regrowth," *IEEE Microwave Guided Wave Lett.*, vol. 7, pp. 192–193, July 1997.

[4] N. B. Carvalho and J. C. Pedro, "Multitone frequency-domain simulation of nonlinear circuits in large- and small-signal regimes," *IEEE Trans. Microwave Theory Tech.*, vol. 46, pp. 2016–2024, Dec. 1998.

[5] V. Rizzoli, A. Neri, F. Mastri, and A. Lipparini, "Inexact-Newton harmonic-balance analysis with time-dependent phasors," in *Proc. 28th European Microwave Conf.*, 1998, pp. 261–266.

[6] S. A. Maas, "Two-tone intermodulation in diode mixers," *IEEE Trans. Microwave Theory Tech.*, vol. MTT-35, pp. 307–314, Mar. 1987.

[7] R. S. Virk and S. A. Maas, "Modeling MESFET's for intermodulation analysis of resistive FET mixers," in *IEEE MTT-S Int. Microwave Symp. Dig.*, 1995, pp. 1247–1250.

[8] S. Peng, P. J. McCleer, and G. I. Haddad, "Nonlinear models for the intermodulation analysis of FET mixers," *IEEE Trans. Microwave Theory Tech.*, vol. 43, pp. 1037–1045, May 1995.

[9] S. A. Maas, *Nonlinear Microwave Circuits*. Norwood, MA: Artech House, 1988.

[10] J. C. Pedro and N. B. Carvalho, "A very fast and efficient computation method for nonlinear distortion on uniformly discretized spectra," in *Proc. Telecommun. Conf. II* , 1999, pp. 519–522.

[11] J. A. García, J. C. Pedro, M. L. De la Fuente, N. B. Carvalho, A. Mediavilla, and A. Tazón, "Resistive FET mixer conversion loss and IMD optimization by selective drain bias," *IEEE Trans. Microwave Theory Tech.*, vol. 47, pp. 2382–2392, Dec. 1999.

Uniplanar One-Dimensional Photonic-Bandgap Structures and Resonators

Tae-Yeoul Yun and Kai Chang

***Abstract*—This paper presents uniplanar one-dimensional (1-D) periodical structures, so-called photonic-bandgap (PBG) structures, and defect high-Q resonators for coplanar waveguide, coplanar strip line, and slot line. Proposed uniplanar PBG structures consist of 1-D periodically etched slots along a transmission line or alternating characteristic impedance series with wide band-stop filter characteristics. A stop bandwidth obtained is 2.8 GHz with a stopband rejection of 36.5 dB. This PBG performance can be easily improved if the number of cells or the filling factor is modified in a parametric analysis. Using uniplanar 1-D PBG structures, we demonstrate new high-Q defect resonators with full-wave simulation and measured results. These structures based on defect cavity or Fabry–Perot resonators consist of a center resonant line with two sides of PBG reflectors. They achieve a loaded Q of 247.3 and unloaded Q of 299.1. The proposed circuits should have many applications in monolithic and hybrid microwave integrated circuits.**

***Index Terms*—Band-stop filter, photonic bandgap, resonator, uniplanar.**

I. Introduction

Similarly to the energy bandgap concept in solid-state electronic materials, photonic-bandgap (PBG) materials or photonic crystals provide a means to control lightwave propagation. Although the PBG structure was developed for use at optical frequencies, it is scalable to microwave and millimeter-wave frequencies because the PBG is an electromagnetic bandgap (EBG) [1]. A one-dimensional (1-D) PBG structure can be made by alternating wave impedances, which has been analyzed and applied to several transmission lines and waveguides in microwave engineering to demonstrate stopband and slow-wave characteristics [2]. In this paper, however, the periodicity is referred to as the PBG because ideas of a new 1-D resonator are based on the defect cavity concept [1].

Two-dimensional (2-D) PBG structures published for antenna and microstrip-line applications consisted of periodical air holes, which are micromachined or drilled through the substrate [3], [4]. A most recently reported 2-D PBG structure for microstrip lines was composed of circularly etched holes on the ground plane along the microstrip line without drilling [5]. The periodically etched hole technique avoids the drilling process and makes PBG structures easier to manufacture. Since most electromagnetic fields are confined to the microstrip-line width, 2-D hole structures can be modified to 1-D structures. In addition, use of uniplanar structures has an advantage that only a one-sided photolithography process is required. In this paper, uniplanar 1-D PBG structures for a coplanar waveguide (CPW), coplanar strip line (CPS), and slot-line PBG are designed, as shown in Fig. 1(a).

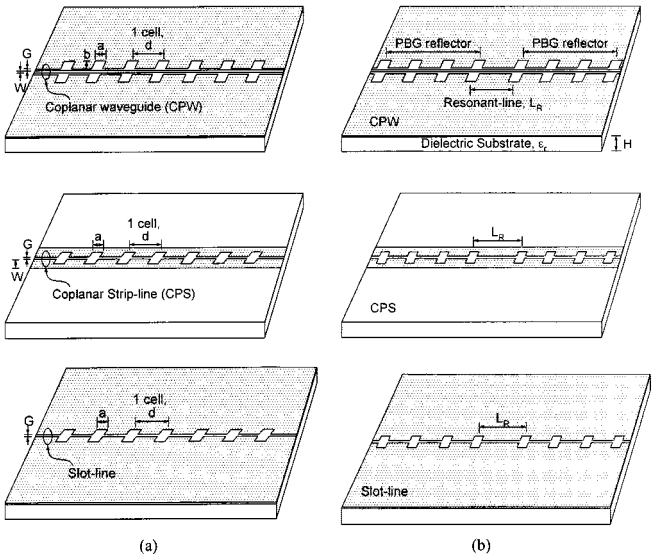

Fig. 1. Uniplanar (CPW, CPS, and slot line) 1-D periodical structures. (a) 1-D PBG bandstop filters. (b) 1-D PBG resonators.

Using the defect cavity concept, 1-D or 2-D optical waveguide resonators with an alternating dielectric constant [6], [7] and image guide resonator [8] have been published for high quality (Q) resonators. Fig. 1(b) shows new CPW, CPS, and slot-line uniplanar resonators using 1-D PBG structures [9]. These resonators consist of a center resonant-line (defect) with periodic PBG reflectors on both sides to implement Fabry–Perot resonators. Two important parameters are analyzed and full-wave simulation and measured results are presented. The uniplanar defect resonators can be readily implemented in monolithic microwave integrated circuits (MMICs) in which loss compensation circuits with active devices can be used.

II. Design and Parametric Analysis

The PBG structure is basically a periodical structure that satisfies the following equation, and strongly shows band-stop filter characteristics as the number of cells is increased [1]:

$$k = \frac{\pi}{d} \tag{1}$$

where k is the propagation constant. The cell distance (d) is equal to 1/2 guided wavelength (λ_g) if k is equal to $2\pi/\lambda_g$. The propagation constant is difficult to determine and full-wave analysis is necessary to calculate λ_g for the structures in Fig. 1. As a simple approximation, it is acceptable to set the propagation constant as approximately the same as an unperturbed transmission line, assuming that the perturbation of the PBG structure is very small [5]. The circuit length is dependent on the cell number, center frequency, and dielectric constant. In this study, the substrate used is a RT/Duroid 6010.5, with relative dielectric constant (ε_r) of 10.5, height (H) of 50 mil, and length of 2 in. The stopband center or resonant frequency (f_o) is chosen near 10 GHz and, thus, the

Manuscript received September 7, 1999. This work was supported in part by the State of Texas Higher Education Coordinating Board under their Advanced Technology Program.

The authors are with the Department of Electrical Engineering, Texas A&M University, College Station, TX 77843-3128 USA (e-mail: tyyun@ee.tamu.edu; chang@ee.tamu.edu).

Publisher Item Identifier S 0018-9480(01)01692-1.